

Journal Pre-proof

Solar thermal performance of two innovative configurations of air-vacuum layered triple glazed windows

Yueping Fang, Saim Memon, Jingqing Peng, Mark Tyrer, Tingzhen Ming



PII: S0960-1481(19)31987-1

DOI: <https://doi.org/10.1016/j.renene.2019.12.115>

Reference: RENE 12824

To appear in: *Renewable Energy*

Received Date: 16 August 2019

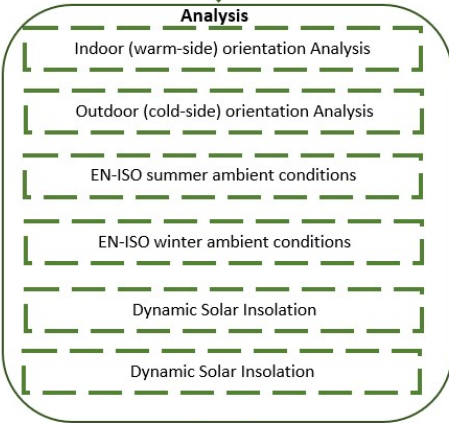
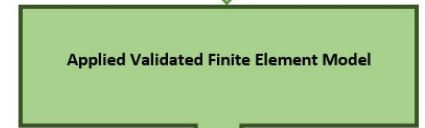
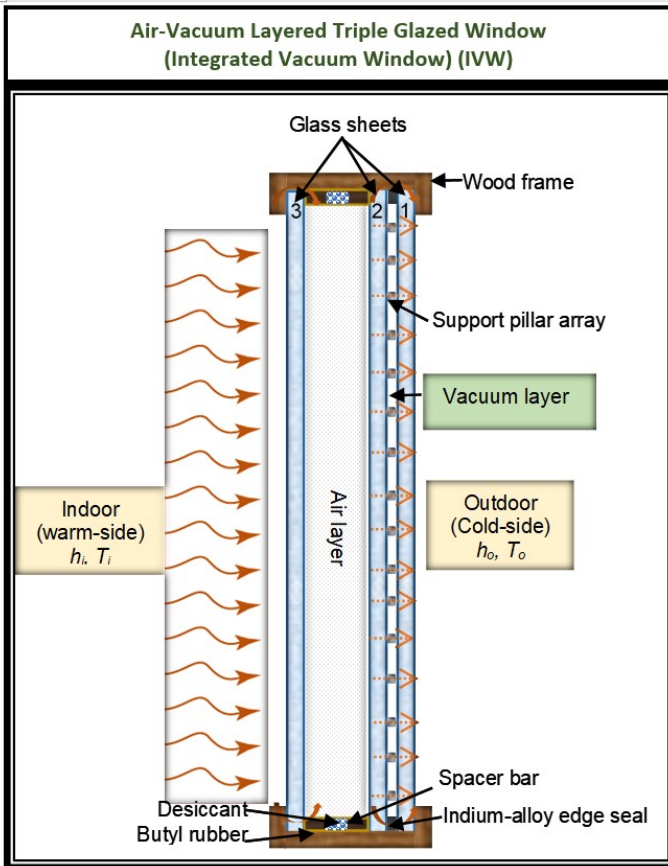
Revised Date: 20 December 2019

Accepted Date: 24 December 2019

Please cite this article as: Fang Y, Memon S, Peng J, Tyrer M, Ming T, Solar thermal performance of two innovative configurations of air-vacuum layered triple glazed windows, *Renewable Energy*, <https://doi.org/10.1016/j.renene.2019.12.115>.

This is a PDF file of an article that has undergone enhancements after acceptance, such as the addition of a cover page and metadata, and formatting for readability, but it is not yet the definitive version of record. This version will undergo additional copyediting, typesetting and review before it is published in its final form, but we are providing this version to give early visibility of the article. Please note that, during the production process, errors may be discovered which could affect the content, and all legal disclaimers that apply to the journal pertain.

© 2019 Elsevier Ltd. All rights reserved.



Journal

Solar thermal performance of two innovative configurations of air-vacuum layered triple glazed windows

Yueping Fang^{a*}, Saim Memon^b, Jingqing Peng^c, Mark Tyrer^a, Tingzhen Ming^d

^a Coventry University, Centre for Research in Built and Natural Environment, School of Energy, Construction and Environment, Priory Street, Coventry, CV1 5FB, UK

^b London South Bank University, London Centre for Energy Engineering, School of Engineering, 103 Borough Road, London, SE1 0AA, UK

^c Hunan University, Key Laboratory of Building Safety and Energy Efficiency of the Ministry of Education, Changsha 410082, P.R. China

^d Wuhan University of Technology, School of Civil Engineering and Architecture, 122 Luoshi Road, Hongshan District, Wuhan 430070, P.R. China

*Corresponding Author: Yueping Fang

Address: Coventry University, Centre for Research in Built and Natural Environment, School of Energy, Construction and Environment, Priory Street, Coventry, CV1 5FB, UK

Email: yueping.fang@coventry.ac.uk

33 Abstract

34

35 This study reports the optimal solar thermal performance of two innovative configurations of air-
36 vacuum layered triple glazed window or Integrated Vacuum Window (IVW). These are when the
37 vacuum layer of IVW is facing the warm or indoor side, i.e. IVW_{warm} , and when the vacuum layer
38 of IVW is facing the cold or outdoor side, i.e. IVW_{cold} , positions at dynamic solar insolation under
39 winter and summer EN-ISO standard ambient conditions. A theoretically and experimentally
40 validated finite element model is employed. The results show that in winter conditions, although
41 the U-value of IVW_{warm} of $0.33 \text{ Wm}^{-2}\text{K}^{-1}$ is lower than that of IVW_{cold} of $0.49 \text{ Wm}^{-2}\text{K}^{-1}$, the IVW_{cold}
42 has a higher solar heat gain. In sunny winter conditions, IVW_{cold} provides higher energy efficiency
43 while in winter night, IVW_{warm} provides higher energy efficiency than IVW_{cold} . The results show
44 that in summer conditions the U-value of IVW_{warm} and IVW_{cold} are $0.34 \text{ Wm}^{-2}\text{K}^{-1}$ and $0.51 \text{ Wm}^{-2}\text{K}^{-1}$
45 respectively, while IVW_{warm} provides lower cooling-load and higher energy-efficiency compared to
46 IVW_{cold} . It is concluded that setting the vacuum gap at the indoor side position provides lower
47 cooling-load and higher energy-efficiency compared to setting the vacuum cavity at the outdoor
48 side position in summer ambient conditions.

49

50 **Keywords:** Vacuum; window; solar insolation; thermal performance; low emittance coatings

51

52 1. Introduction

53

54 A significant rise of the sustainable development of buildings [1] with a goal of Nearly Zero-
55 Energy Building (NZEB) [2] is emerged by merging the progressive technologies of PV, Wind and
56 optimal building fabric insulation with a future leading to the idea of Generating-Energy Building
57 (GEB). To achieve this long-term sustainable development goal, a number of retrofitting
58 measures have already been reported [3] and it is found that usually the windows exhibit poorer
59 thermal performance [4] and poorer sound insulation among other components since windows
60 need to allow the sunlight get into the rooms and the occupants to view outside. Heat loss
61 through windows take place by conductive, convective and radiative heat transfers [5]. Multiple
62 glass sheets with an air or inert gas filled gap, enclosing the air and inert gas in between, can
63 reduce the conductive heat loss across the glazing. Low-emittance (low-e) coatings can be
64 applied to the inner surfaces between two sheets of glass to decrease the radiative heat transfer
65 between these two inner surfaces [6, 7]. The width of gas-filled gap(s) requires typically about 10
66 mm, otherwise the contribution of heat transfer resulting from gas conduction and convection will
67 compromise the thermal insulation of the gas-filled window [8]. The multiple glass sheets with
68 gas-filled gaps increases the thickness and weight as well as reduce the light transmission.
69 Vacuum glazed window overcomes these difficulties [9]. Vacuum glazed window combines the
70 merits of lower thermal transmittance (U value) $< 1 \text{ Wm}^{-2}\text{K}^{-1}$ with higher solar heat gains (g-value
71 > 0.76) whilst maintaining the visual light transmittance of about 0.74 [10]. It comprises an
72 evacuated cavity between two glass sheets sealed contiguously along their perimeter. Low-

73 emissivity coatings are coated onto either one or two inner glass surfaces inhibit long-wave
74 radiation. The vacuum pressure of 0.1 Pa within the vacuum cavity enclosed by the two sheets of
75 glass is achieved by evacuating with specialised made vacuum cup connected to the turbo-
76 molecular vacuum pump [11, 12], it reduces the thermal conduction and convection to minimum
77 level except the heat transfer via support pillars and edge seal. The edge seal width of air-filled
78 layer and vacuum layer are 10 mm and 0.12 mm respectively. However, the vacuum glazing
79 adds the benefits of a very small gap can be integrated to the conventional air-filled glazing with
80 the existing window frames for the retrofit as well as for new window frames [4].

81
82 The first successful vacuum glazing [13] utilises high-temperature sealing material, lead-based
83 solder glass from Schott Glass company [14], to seal the edges hermetically at 450 °C. The group
84 at the Ulster University developed the successful low-temperature edge sealing method (160 °C),
85 utilising indium-alloy [6], to seal the edges of the glass sheets and added benefits of incorporated
86 low-e coatings and the use of tempered glass. Since then, a significant development has been
87 made in the vacuum edge sealing materials for the fabrication and development of vacuum
88 glazing and triple vacuum glazing [15, 16]. Fang et al (2014) [4] has shown that vacuum glazing
89 can be fabricated at temperatures around 160 °C, thus removing the thermal restriction on the
90 use of tempered glass [17]. Thus, subject to outgassing characteristics, the full range of optical
91 glazing properties currently seen in gas filled glazing may also be possible with evacuated
92 cavities. Although significant efforts have been made by many researchers [18, 19], the U-value
93 of the vacuum glazing has been reduced close to the theoretical limits. To meet the demand of
94 Nearly Zero-Energy Buildings, triple vacuum glazing (TVG), hybrid vacuum glazing (HVG) and
95 Integrated Vacuum Window (IVW) can further improve the window performance. The difference
96 between HVG and IVW is that HVG uses argon gas and does not account the frame whilst IVW
97 does use air and account the frame. Preliminary research have been undertaken by the
98 researchers [20, 15]. The predicted U-values of TVG and HVG have been experimentally
99 validated [21].

100
101 Recently, there has been an increasing mass production, such as Qingdao Hengda Vacuum
102 Glass Ltd [22], LandVac Ltd. [23], and Panasonic Ltd [24], and installation of vacuum glazing in
103 Nearly Zero-Energy Buildings in China and Japan. The NSG SPACIA Hybrid vacuum glazing [25]
104 utilises the argon gas filled layer and solder-glass based vacuum glazing and there have been
105 issues of argon gas leakage and its added complexity of the secondary edge seal. In this paper,
106 air-vacuum layered triple glazed window is developed with low-temperature (indium-alloy) edge
107 seal for vacuum layer and butyl rubber seal for air-filled layer, named as Integrated Vacuum
108 Window (IVW), that added the benefits of incorporating the low-e coatings and temperature
109 sensitive heat-reflective coatings. This paper offers for the first time, current industrial knowledge
110 gap, of understanding the optimal indoor(warm-side) / outdoor (cold-side) position of the vacuum
111 layer of IVW under winter and summer ambient EN-ISO conditions at dynamic solar insolation for
112 the greater benefit in terms of maintaining the durability and longevity of vacuum edge-seal, the

113 position of vacuum layer in IVW, a possibility of reducing the condensation issue by reducing the
114 edge effects and additional temperature differential based internal and external tensile stresses.
115 This paper also reports the solar thermal performance of IVW subjected by various solar
116 insolation under EN-ISO winter and summer ambient conditions [26, 8]. The optimal setting
117 method of IVW is presented based on the analysis using validated [7] finite element model.

118

119 **2. Methodology**

120 Integrated Vacuum Window (IVW), as shown in Fig. 1, comprises three glass sheets, each
121 dimensions of 400 mm x 400 mm x 4 mm, having a layer of air-filled gap and a layer of vacuum
122 gap supported with a wooden frame. The advantages of IVW as compared to the low-
123 temperature indium-alloy sealed vacuum glazing (VG) are: i) its U-value is lower than VG due to
124 the added air gap, which contributes to the added thermal resistance within the IVW; ii) the stress
125 within the VG is significantly reduced, since the added air gap enclosed by the 3rd glass sheet
126 reduces the temperature differential between the two sheets of glass of IVW, thus improving the
127 durability and longevity of the vacuum layer; iii) the third glass sheet and the air gap, reduce the
128 risk of condensation at the edge seal area of the Vacuum layer due to the thermal bridge of the
129 edge seal. The thermal performance of IVW has been analysed using an experimentally validated
130 finite element model (FEM) [7, 10, 21] in which the solar thermal performance of IVW with
131 different positions of the vacuum layer subjected to various levels of solar insolation were
132 investigated in this work.

133

134

135

136

137

138

139

140

141

142

143

144

145

146

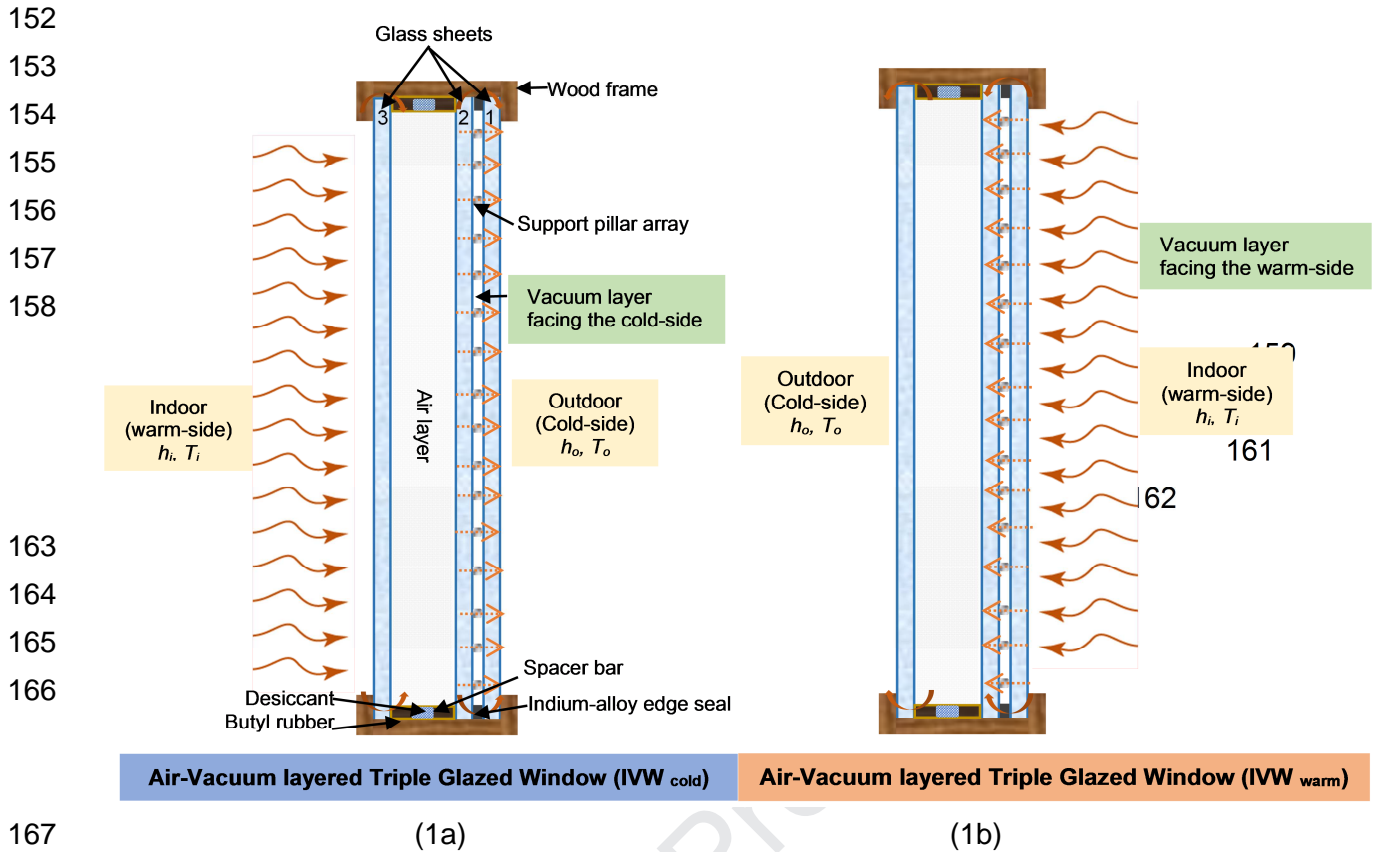
147

148

149

150

151



167
168 **Fig.1** Schematic diagram of air-vacuum layered triple glazed window in which vacuum layer is
169 facing the EN-ISO ambient conditions of: (1a) outdoor (cold-side) named as (IVW_{cold}) and (1b)
170 indoor (hot-side) named as (IVW_{warm}). (The diagram is not to scale)

171

172 2.1 Analytic model of Integrated Vacuum Window (IVW)

173 An analytic heat transfer model for IVW has been established following experimentally and
174 theoretically validated approach of [7, 10, 21]. Due to the geometrical symmetry of the IVW and to
175 reduce the computational time, one-fourth of the IVW is modelled. The equivalent thermal
176 resistive network for the one-fourth of a support-pillar, due to the symmetry of the circular shape
177 of the support-pillar, and to reduce the computational time one quarter of the IVW is modelled
178 and is consistent to the validated approach, as shown in Fig. 2.

179
180
181
182
183
184
185

186

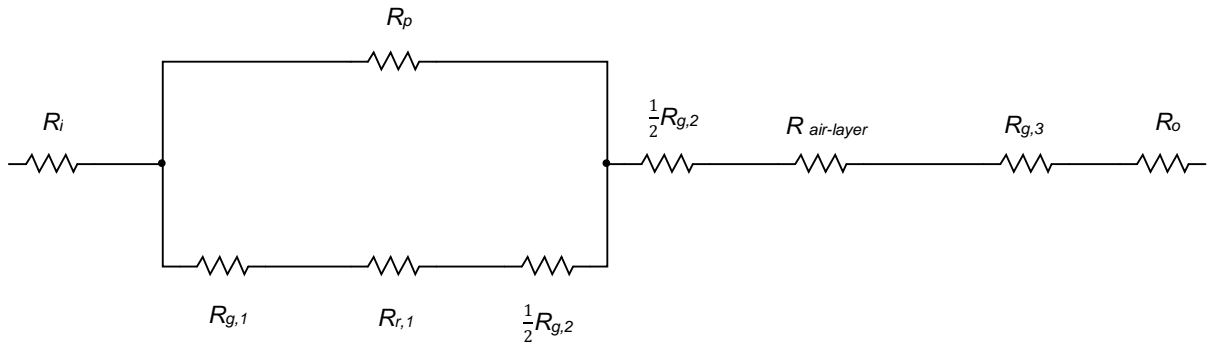
187

188

189

190

191



192 **Fig. 2** An equivalent thermal 192 resistance circuit diagram of the quarter cell unit
 193 with a quarter of a pillar at the symmetric centre of the unit.

194

195 The overall thermal resistance across the IVW is determined by Eq. (1),

196

$$197 \quad R_{total} = \frac{R_p(R_{g,1} + R_{r,1} + \frac{1}{2}R_{g,2})}{R_p + R_{g,1} + R_{r,1} + \frac{1}{2}R_{g,2}} + \frac{1}{2}R_{g,2} + R_{air-layer} + R_{g,3} \quad (1)$$

198

199 Where R_p is the thermal resistance of the support pillar, determined by Eq. (2) [13]

200

$$201 \quad R_p = \frac{1}{2\lambda_g a} \quad (2)$$

202

203 $R_{g,1}$, $R_{g,2}$, $R_{g,3}$ are thermal resistances of three glass sheets 1, 2 and 3, determined by Eq. (3),

204

$$205 \quad R_{g,m} = \frac{d_m}{\lambda_g A} \quad (3)$$

206

207 where d_m is the glass thickness; m is either *I*, or *II*, or *III*; a is support pillar's radius; A

208 indicates the unit cell area (so $A = \rho^2$); λ_g is glass thermal conductivity.

209

210 The thermal resistance against radiative heat transfer between the two inner surfaces of glass

211 panes enclosing the air filled gap and vacuum cavity is given by Eq. (4).

212

$$213 \quad R_{r,n} = \left(\frac{1}{\varepsilon_x} + \frac{1}{\varepsilon_y} \right) (4\sigma T_{xy}^3 A)^{-1} \quad (4)$$

214

215 In the equation ε_x and ε_y indicate the atmospheric emittance of two inner surfaces x and y within

216 the vacuum cavity and air filled gap; T_{xy} is the mean temperature of the two sheet of glass

217 enclosing either the vacuum gap or the air filled gap; σ stands for Stefan-Boltzmann constant.

218

219 The thermal resistance of the air filled gap $R_{air,gap}$ is computed by the thermal resistance R_{air}
 220 against conductive and convective heat flow across the air filled gap and the thermal resistance
 221 R_r against radiative heat flow within the air gap enclosed by two sheet of glass, i.e.

$$222 \quad R_{air,gap} = \frac{R_{air}R_{r,2}}{R_{air}+R_{r,2}} \quad (5)$$

$$224 \quad R_{air} = \frac{1}{Ah_{air,gap}} \quad (6)$$

226 The British and European standard BS EN 673 [26] recommends that

$$227 \quad h_{air} = Nu \frac{\lambda}{s}$$

$$229 \quad h_{air} = Nu \frac{k}{l} \quad (7)$$

231 Here, l is the air gap width; Nu indicates the Nusselt number; k indicates the air thermal
 232 conductivity:

$$233 \quad Nu = K \cdot (Gr \cdot Pr)^n \quad (8)$$

235 In Eq. (8), K is a constant; n : an exponent; Pr : the Prandtl number; Gr : the Grashof number;

$$236 \quad Gr = \frac{9.81s^3 \Delta T \cdot \rho^2}{T_a \mu^2} \quad (9)$$

$$238 \quad Pr = \frac{\mu c}{k} \quad (10)$$

240 Here, ΔT stands for the temperature differential between surfaces 2 and 3 in Fig. 1(a) and
 241 surfaces 4 and 5 in Fig. 1(b) of the air gap. For the air in the air gap, μ is the dynamic viscosity;
 242 T_a : the mean temperature of the two inner surfaces of sheet of glass enclosing the air gap; c : the
 243 specific heat capacity; ρ : the density. If Nu is less than 1, then the Nu number is selected to be 1.
 244 For air gap between the two vertical glass sheets: K is chosen to be 0.035, n chosen to be 0.38
 245 [26]. The R_i and R_o are thermal resistance of the indoor and outdoor surface of IVW. The overall
 246 U-value of the IVW is then determined by Eq. (11).

$$247 \quad U_{a-a,tot} = \frac{1}{(R_i + R_{tot} + R_o)A} \quad (11)$$

248 The heat flow across the whole IVW is calculated by adding the heat flow through the central
 249 section of IVW with the heat transfer across the edge seal of the vacuum cavity and the spacer of
 250 air filled gap.
 251
 252

253 2.2 Finite Element Model

254 The validated boundary conditions for the finite element model are detailed as follows:

- 255
- 256 a) The overall heat loss coefficients of the outdoor and indoor surfaces of IVW are $h_o = 25$
 257 $\text{Wm}^{-2}\text{K}^{-1}$ and $h_i = 7.7 \text{Wm}^{-2}\text{K}^{-1}$. [8]
- 258
- 259 b) The temperatures of outdoor and indoor ambient are $0\text{ }^\circ\text{C}$ and $20\text{ }^\circ\text{C}$ respectively. [8]

260

261 The Galerkin approach was used to discretize and solve the governing equation. The radiation
 262 between the two parallel surfaces of the finite element brick within the vacuum and air gaps is
 263 determined by Eq. (12).

$$264 \quad dQ_r = \left(\frac{1}{\varepsilon_j} + \frac{1}{\varepsilon_k} - 1\right)^{-1} (4\sigma T_{j,k}^3 dA_v)(T_j - T_k) \quad (12)$$

266 Here, dA_v is determined by Eq. (13).

$$267 \quad dA_v = dx dy \quad (13)$$

270

271 The dQ_r was integrated with the conductive heat transfer across the support pillar in the vacuum
 272 cavity and the air-filled gap. The heat flow across the air-filled gap was simplified to the heat
 273 conduction through an equivalent material with an effective thermal conductivity [27] determined
 274 by Eq. (14) which is the effective air gap thermal conductivity.

$$275 \quad k = \frac{s}{A_g R_{air,gap}} \quad (14)$$

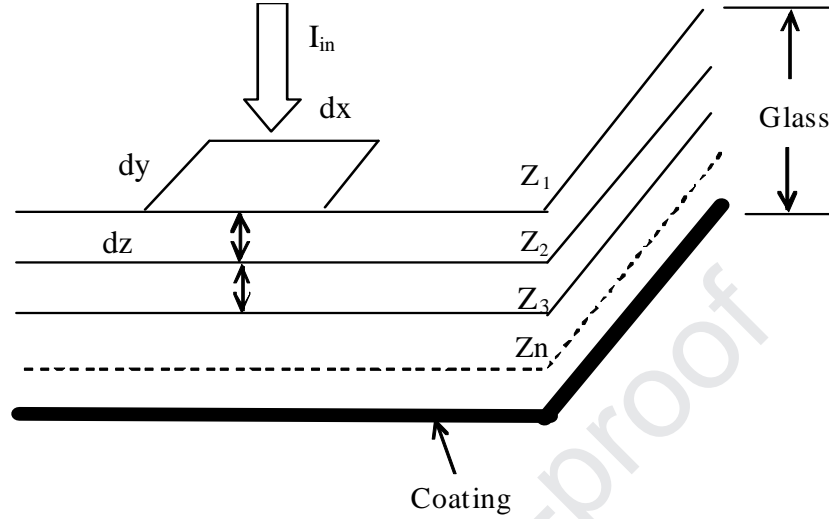
277 Here, s is the air gap width and A_g is the glass sheet area.

278

279 The circular support pillars with diameter of a are integrated into the model as a cubic pillar with
 280 width of $\sqrt{\pi}a$ and with the physical properties of stainless [10-12]. The area (cross-sectional) of
 281 the circular pillar and cubical pillar are same, and therefore conduct same amount of heat under
 282 the same ambient conditions [15]. The mesh numbers within and around the pillar are denser to
 283 achieve higher accuracy than that of the area distance away from the pillars to reduce the CPU
 284 running time [7].

285

286 The edge spacer and butyl rubber seal of double glazing was simplified as a single equivalent
 287 materials with effective thermal conductivity of $0.16 \text{ Wm}^{-2}\text{K}^{-1}$ that was determined by a 2-D finite
 288 element model detailed by [10, 21].



302 **Fig. 3** Schematics of an enlarged finite element volume within the glass sheet. The diagram is not
 303 to scale.

304 Solar energy absorption in each finite volume is shown in Fig. 3 and is given by Eq. (15).

$$305 \quad dI_{absorbed} = I_{in}(I_z - I_{z+1})dxdy \quad (15)$$

306 where I_z and I_{z+1} are the solar insolation intensities at the up and bottom surfaces of each finite
 307 element, which was given by Eq. (16).

$$308 \quad I_L = 1 - e^{-C_e Z_L} \quad (16)$$

309 where the glass extinction coefficient, C_e is a parameter indicating the amount the glass absorbs
 310 solar radiation [28]. It has been reported that the extinction coefficient of “greenish edge” glass is
 311 32 m^{-1} and that of “white edge” glass is 4 m^{-1} . In this finite volume model, C_e was selected to be
 312 30 m^{-1} . Z_L is the length of the sun light passing within the IVW from the outdoor glass surface.

313 3. Results and Discussion

314 3.1 Solar thermal performance of IVW under EN-ISO winter boundary conditions

315 The isotherms of IVW_{warm} and IVW_{cold} settings, as shown in Fig. 1, under standard winter ambient
 316 conditions [8] with solar insolation of 0 W/m^2 and 300 Wm^{-2} are presented in Fig. 4 and Fig. 5.

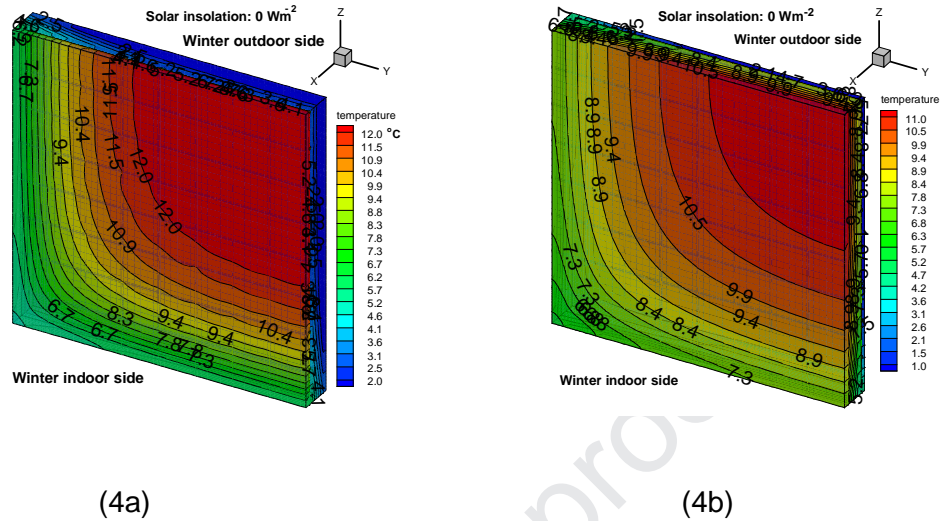


Fig. 4 3D Isotherms of (4a) IVW_{warm} with the vacuum cavity at the indoor (warm-side) and (4b) IVW_{cold} with the vacuum cavity at the outdoor (cold-side) at the solar insolation of 0 W/m^2 .

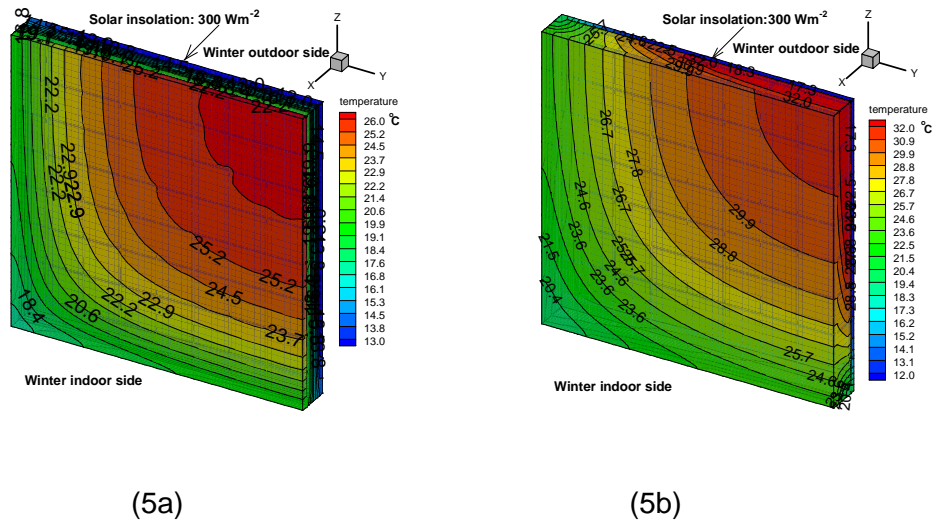


Fig. 5 3D Isotherms of (5a) IVW_{warm} with the vacuum cavity at the indoor (warm-side) and (5b) IVW_{cold} with the vacuum cavity at the outdoor (cold-side) at the solar insolation of 300 W/m^2 .

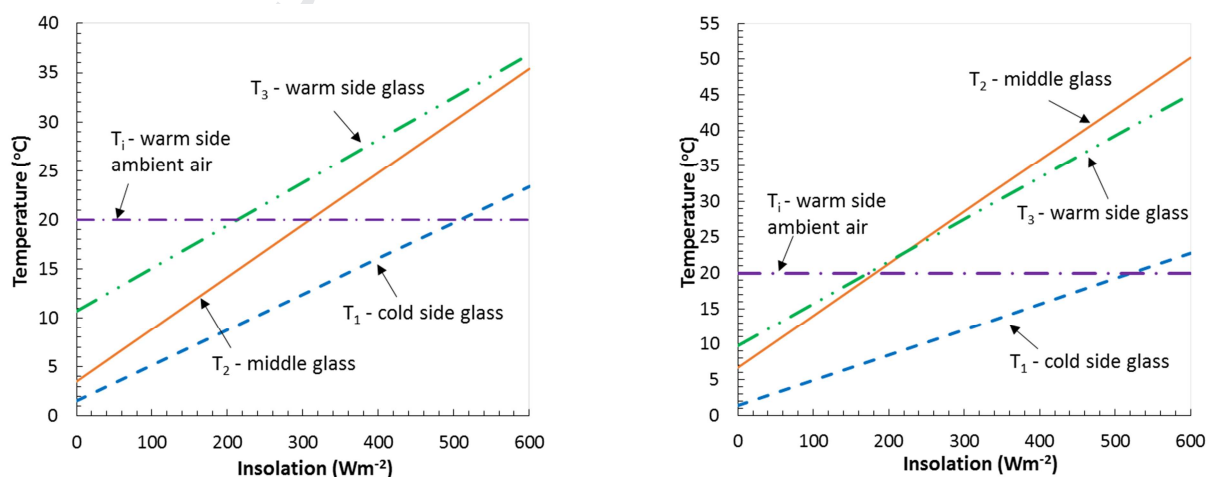
In Fig. 4 with solar insolation of 0 Wm^{-2} , the temperatures at the central glazing area of IVW_{warm} and IVW_{cold} are $12.6 \text{ }^\circ\text{C}$ and $11.1 \text{ }^\circ\text{C}$. Their U-values are $0.33 \text{ Wm}^{-2}\text{K}^{-1}$ and $0.49 \text{ Wm}^{-2}\text{K}^{-1}$ respectively. The vacuum cavity at the indoor warm side of the middle glass reduces the heat transfer more effectively than that at the cold outdoor side. The air gap at the indoor side of the middle glass exhibits higher thermal conductance compared to that when the air gap is at the

359 outdoor low temperature side, since higher temperature at the indoor warm side leading to a
 360 higher heat convection within the air gap. This means that at night or on overcast winter days,
 361 IVW_{warm} provides better insulation than IVW_{cold} , i.e. less heat loss.

362
 363 Fig. 4(a) and Fig. 5(a) show that with solar insolation increasing from 0 to 300 Wm^{-2} , the
 364 temperature at the centre of the indoor warm side glass of IVW_{warm} increases from $12.6 \text{ }^\circ\text{C}$ to 25.5
 365 $^\circ\text{C}$; while in Fig. 4(b) and Fig. 5(b), the temperatures of the central glazing section of the indoor
 366 glass sheet of IVW_{cold} increases from $11.1 \text{ }^\circ\text{C}$ to $30.4 \text{ }^\circ\text{C}$, i.e. the temperature increase in the
 367 indoor glass of IVW_{cold} is higher than that of IVW_{warm} . This is because in IVW_{cold} , the vacuum
 368 cavity at the cold side provides better insulation compared to that when the air gap is at the cold
 369 side as in IVW_{warm} , thus reduces the heat transfer from the middle sheet of glass to the sheet of
 370 glass at the cold side more effectively compared to that in IVW_{warm} with the vacuum cavity being
 371 at the warm side. This means that subjected to solar insolation, IVW_{cold} transfers more heat into
 372 the warm ambient side, given the temperature of indoor side glass is over the indoor ambient
 373 temperature and thus has a higher solar heat gain than IVW_{warm} .

374
 375 Fig. 4 and Fig. 5 also show that the temperatures of the indoor glass edge area is lower compare
 376 to that at the area of central glazing, because more heat is transferred by conduction across the
 377 seal of vacuum cavity and the spacer of air gap from the warm indoor environment to the outdoor
 378 environment compared to the heat flow across the central window area because of higher
 379 insulation of the vacuum cavity.

380
 381 The temperature variations of three glass sheets of IVW_{warm} and IVW_{cold} subjected to various
 382 levels of solar radiation were calculated by using the validated FEM model as shown in Fig. 6.
 383



392

393 (6a)

(6b)

394 **Fig. 6** Surface Temperatures in relation to dynamic solar insolation of (6a) IVW_{warm} and (6b)
 395 IVW_{cold} .

396

397 Fig. 6a shows an increase of solar insolation higher than 210 W/m^2 , the indoor glass temperature
 398 T_3 is higher compared to indoor ambient temperature T_i of $20 \text{ }^\circ\text{C}$ and middle glass sheet
 399 temperature T_2 , the warm-side glass sheet transfers heat onto both the warm-side ambient air
 400 and into the middle sheet of glass and then to the glass sheet at the cold side. Fig. 6b shows that
 401 with an increase of solar insolation, the middle glass sheet temperature T_2 is increased faster
 402 than that of indoor glass sheet temperature T_3 ; T_2 becomes higher than T_3 when the solar
 403 insolation increases to 200 W/m^2 since the heat absorbed from solar energy is difficult to transfer
 404 to the outdoor glass sheet because of the lower thermal conductance of the vacuum cavity at the
 405 outdoor side. Heat flows from the middle sheet of glass to the indoor sheet of glass, then to the
 406 indoor warm ambient, due to the indoor glass temperature being higher compared to the indoor
 407 ambient temperature.

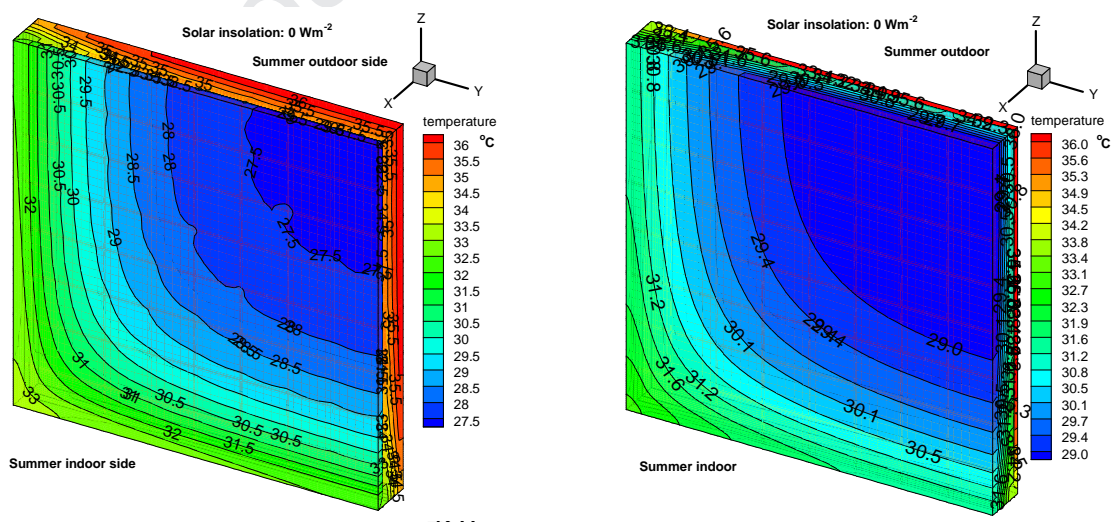
408

409 3.2 Solar thermal performance of IVW under EN-ISO summer boundary conditions

410 The employed summer boundary conditions for the finite element model are listed as follows: the
 411 overall heat loss coefficients of the outdoor and indoor IVW surfaces are $h_o = 25 \text{ Wm}^{-2}\text{K}^{-1}$ and $h_i =$
 412 $7.7 \text{ Wm}^{-2}\text{K}^{-1}$; the outdoor and indoor ambient temperature: $37 \text{ }^\circ\text{C}$ and $22 \text{ }^\circ\text{C}$ [8]. The isotherms of
 413 IVW_{warm} and IVW_{cold} without solar insolation and with insolation of 300 W/m^2 are presented in
 414 Figs. 7 and Fig. 8.

415

416



426

427

(7a)

(7b)

428 **Fig. 7** 3D Isotherms of (7a) IVW_{warm} with the vacuum cavity at the indoor (warm-side) and (7b)
 429 IVW_{cold} with the vacuum gap at the outdoor (cold-side) at the solar insolation of 0 W/m^2 .

430

431

432

433

434

435

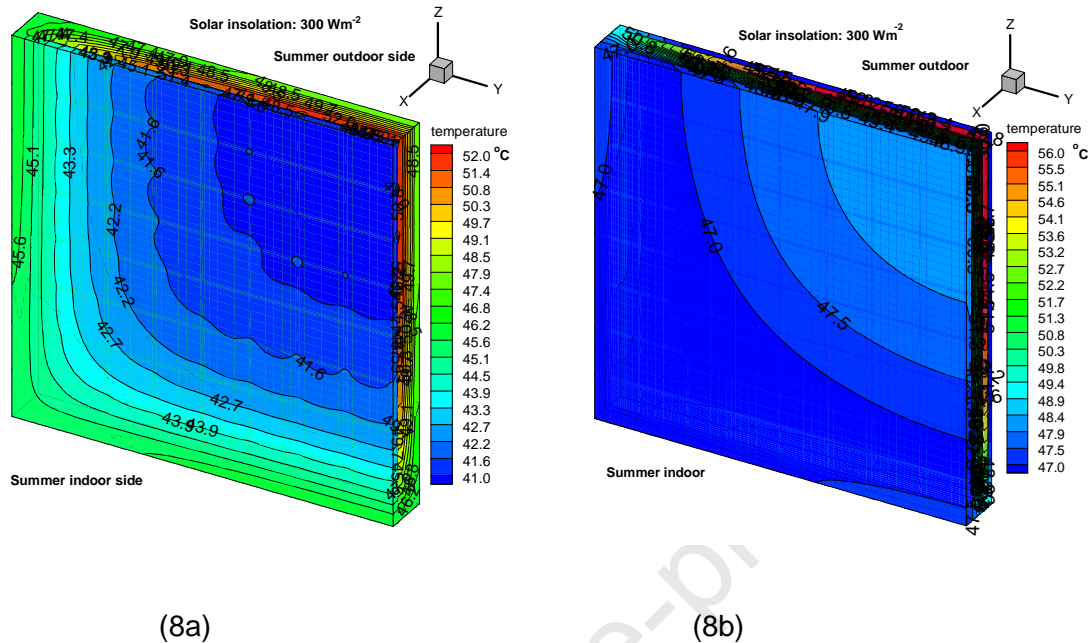
436

437

438

439

440



441 **Fig. 8** 3D Isotherms of (8a) IVW_{warm} with the vacuum cavity at the indoor (warm-side) and (8b)
 442 IVW_{cold} with the vacuum cavity at the outdoor (cold-side) at the solar insolation of 300 W/m^2 .

443 Fig. 7 shows that with solar insolation of 300 W/m^2 , the temperatures at the centre of the indoor
 444 (cold-side) glass sheets of IVW_{warm} and IVW_{cold} are $27.7 \text{ }^\circ\text{C}$ and $29.5 \text{ }^\circ\text{C}$. Their U-values are 0.34
 445 $\text{Wm}^{-2}\text{K}^{-1}$ and $0.51 \text{ Wm}^{-2}\text{K}^{-1}$ respectively. The vacuum cavity at the indoor cool side of the middle
 446 glass of IVW_{warm} reduces the heat transfer more effectively than that when the vacuum cavity is at
 447 the outdoor warm side of the middle sheet of glass. The heat absorbed by the middle sheet of
 448 glass cannot transfer into the indoor glass sheet due to high insulation of vacuum cavity of
 449 IVW_{warm} . For IVW_{cold} , the heat absorbed by the middle sheet of glass can easily transfer into the
 450 indoor glass due to higher thermal conductance of air gap at the indoor side of middle glass
 451 sheet. Thus, the temperature of indoor glass of IVW_{cold} is higher compared to that of indoor sheet
 452 of glass of IVW_{warm} , resulting in the temperature of indoor sheet of glass of IVW_{cold} being higher
 453 compared to that of IVW_{warm} .

454

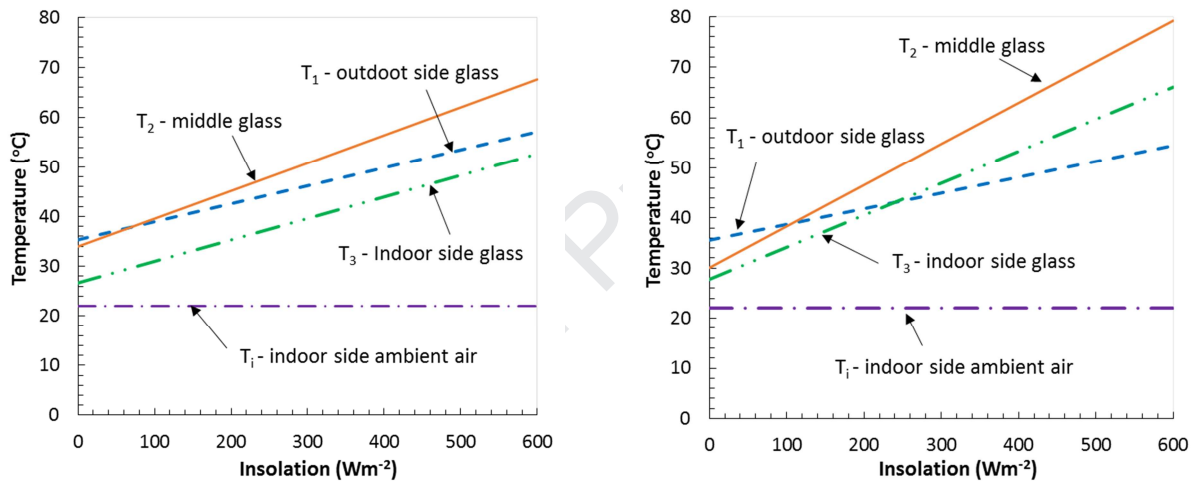
455 Fig. 7(a) and Fig. 8(a) show that an increase of solar insolation from 0 to 300 W/m^2 , the
 456 temperature of the indoor central glazing area of IVW_{warm} increases from $27.7 \text{ }^\circ\text{C}$ to $40.0 \text{ }^\circ\text{C}$,
 457 whilst in Fig. 7(b) and Fig. 8(b), the temperatures of the central glazing section of the indoor
 458 cooler glass of IVW_{cold} increases from $29.5 \text{ }^\circ\text{C}$ to $47.0 \text{ }^\circ\text{C}$, i.e. the increase in temperature of the
 459 indoor (cold-side) glass sheet of IVW_{cold} is higher than that of IVW_{warm} . This is because in IVW_{cold} ,
 460 the vacuum gap at the outdoor side provides better insulation than the air gap at the outdoor side
 461 as in IVW_{warm} , thus decreases the heat flow from the middle sheet of glass to the outdoor
 462 environment more effectively compared to that in IVW_{warm} . This causes the temperature of the

463 indoor sheet of glass increasing faster than that when the vacuum gap is at the indoor side of the
 464 middle glass sheet of IVW_{warm} , thus IVW_{cold} transfers more heat into the indoor ambient than
 465 IVW_{warm} , providing a higher solar heat gain than IVW_{warm} , leading to a higher cooling load
 466 compared to IVW_{warm} .

467
 468 Figs 7 and 8 also show that the temperature of the indoor sheet of glass near the edge area is
 469 higher than that of central glazing area, since more heat is conducted via both the seal of vacuum
 470 cavity and spacer of the air gap from the warm outdoor environment compared to the heat flow
 471 across the central window area because of higher insulation of the vacuum cavity.

472
 473 The temperature variations of three glass sheets of IVW_{warm} and IVW_{cold} subjected to various
 474 levels of solar radiation were determined using the FEM as shown in Fig. 9.

475



477 (9a)

(9b)

478 **Fig. 9** Surface temperatures of the three glass sheets of (9a) IVW_{warm} and (9b) IVW_{cold} subjected
 479 to various solar insolation.

480
 481 Fig. 9(a) shows that when the solar insolation is higher than 60 W/m^2 , the surface temperature T_2
 482 of the middle glass sheet is taking over temperature T_1 of indoor side glass thus the heat
 483 absorbed by the middle glass transfers to the outdoor glass, then to the outdoor ambient
 484 environment across the air gap. Because of the high insulation of the vacuum cavity at the indoor
 485 side, the heat absorbed by the middle glass sheet transfers into the indoor environment at a
 486 much lower rate than that into the outdoor environment. In a move to Building Integrated PV
 487 technology, if semi-transparent PV cells were to be incorporated then they should be set onto the
 488 indoor (warm-side) of the glass sheet enclosing the vacuum gap, since indoor glass temperature
 489 T_3 is lower than that of outdoor glass temperature T_1 .

490

491 Fig. 9(b) shows that when the solar insolation is higher than 110 W/m^2 , the middle glass
492 temperature T_2 is higher than the outdoor glass sheet temperature T_1 , thus the heat absorbed by
493 the middle glass transfers into the outdoor environment across the vacuum gap, but at a much
494 lower rate than that transfers into the indoor environment across the air gap. IVW_{cold} exhibits a
495 much higher solar heat gain g-value and a higher cooling load than IVW_{warm} . With insolation
496 increasing to 220 W/m^2 , temperature T_3 of the indoor glass is taking over temperature T_1 of
497 outdoor glass, transferring the heat to both indoor ambient and the outdoor glass sheet, then to
498 the outdoor ambient environment.

499

500 In summary, the position that the vacuum layer facing the indoor (warm-side) of the middle glass
501 sheet provides a lower cooling load and higher energy efficiency compared to setting the vacuum
502 cavity at the outdoor side of the middle glass sheet in summer ambient conditions.

503

504 5. Conclusions

505 Thermal performance of IVW subjected to various levels of solar insolation were simulated using
506 a validated finite volume model that has been experimentally and theoretically validated by the
507 previous work. The results show that in the winter EN-ISO ambient condition IVW_{cold} exhibits a
508 larger solar heat gain g-value, transferring more heat into the warm indoor environment, despite
509 the fact that the U-value of IVW_{warm} with the vacuum cavity at the indoor side of the middle sheet
510 of glass being lower than that of IVW_{cold} with the vacuum gap at the cold side. It is concluded that
511 at the IVW_{cold} setting at which the vacuum layer facing the cold-side is preferred during winter
512 daytimes with sufficient solar insolation. However, IVW_{warm} with a lower U-value exhibits better
513 thermal performance during winter nights, i.e. lower heat loss compared to IVW_{cold} . Thus, IVW
514 with a pivotal axial that enables rotation of the window during winter daytime and nighttime may
515 provide optimized energy saving potential.

516

517 Detailed analysis for the energy balance of IVW at different locations on the earth is required to
518 achieve maximized energy efficiency of IVW. For instance, in areas with long winter nights or with
519 short sunny days, IVW_{warm} is better than IVW_{cold} since IVW_{warm} has lower U-value than IVW_{cold} ;
520 while in areas where g-value dominates the energy balance, IVW_{cold} is better than IVW_{warm} since
521 IVW_{cold} has a higher g-value than IVW_{warm} , even if the U-value of IVW_{cold} is higher than that of
522 IVW_{warm} .

523

524 In summer EN-ISO boundary conditions, it is concluded that IVW_{warm} provides lower cooling load
525 compared to IVW_{cold} , since the vacuum gap at the outdoor side of the middle glass sheet of
526 IVW_{cold} more efficiently prevents the heat absorbed by the middle glass sheet transferring into the
527 outdoor ambient compared to the case when vacuum gap is at the indoor side of the middle glass

528 sheet. Thus, IVW_{cold} provides higher solar heat gain compared to IVW_{warm} , which will increase the
529 cooling load of the room in summer.

530

531 As for the future work recommendation, it is pertinent to mention the scope of integrating the
532 Semi-Transparent PV (STPV) cell into IVW. In this case, the results of this paper implicate that
533 STPV should then be set on the external glass sheet of the IVW enclosing the vacuum gap. In
534 this case, the STPV would face the outdoor (cold-side) of IVW_{cold} in winter. During this time
535 period, IVW_{cold} achieves higher solar heat gain. STPV will work at a higher energy transfer
536 efficiency due to lower glass temperature where the STPV is integrated. In the summer time, the
537 STPV should be set on the indoor (warm-side) of IVW_{warm} , since the temperature of indoor glass
538 of IVW_{warm} is lower than that of IVW_{cold} , thus STPV will achieve a higher energy transfer
539 efficiency, and IVW_{warm} can achieve a lower solar heat gain g-value, thus a lower cooling load
540 compared to IVW_{cold} .

541

542

543 **Acknowledgement**

544

545 This work was supported by the Pump-Prime project of Coventry University, InnovateUK project-
546 ICUR grant (13-14) 2018 and the self-initiated UK China industrial research collaboration.

547

548 **References**

549

- 550 [1]. Wu, M.H., Ng, T.S. and Skitmore, M.R., 2016. Sustainable building envelope design by
551 considering energy cost and occupant satisfaction. *Energy for sustainable development*, 31,
552 pp.118-129.
- 553 [2]. D'Agostino, D. and Mazzarella, L., 2018. What is a Nearly zero energy building? Overview,
554 implementation and comparison of definitions. *Journal of Building Engineering*.
- 555 [3]. Memon, S., 2014. Analysing the potential of retrofitting ultra-low heat loss triple vacuum
556 glazed windows to an existing UK solid wall dwelling. *International Journal of Renewable
557 Energy Development*, 3(3), p.161.
- 558 [4]. Fang, Y., Hyde, T.J., Arya, F., Hewitt, N., Eames, P.C., Norton, B. and Miller, S., 2014.
559 Indium alloy-sealed vacuum glazing development and context. *Renewable and Sustainable
560 Energy Reviews*, 37, pp.480-501.
- 561 [5]. Fang, Y., Hyde, T., Hewitt, N., Eames, P.C. and Norton, B., 2009. Comparison of vacuum
562 glazing thermal performance predicted using two-and three-dimensional models and their
563 experimental validation. *Solar Energy Materials and Solar Cells*, 93(9), pp.1492-1498.
- 564 [6]. Eames, P.C., 2008. Vacuum glazing: current performance and future
565 prospects. *Vacuum*, 82(7), pp.717-722.
- 566 [7]. Griffiths, P.W., Eames, P.C., Hyde, T.J., Fang, Y. and Norton, B., 2006. Experimental
567 characterization and detailed performance prediction of a vacuum glazing system fabricated
568 with a low temperature metal edge seal, using a validated computer model. *Journal of solar
569 energy engineering*, 128(2), pp.199-203.

- 576
577 [8]. EN ISO 10077-1. 2017. Thermal performance of windows, doors, and shutters – calculation
578 of thermal transmittance –part 1: simplified method. Brussels: European Committee for
579 standardization (CEN).
580
- 581 [9]. Memon, S., Fang, Y. and Eames, P.C., 2019. The influence of low-temperature surface
582 induction on evacuation, pump-out hole sealing and thermal performance of composite
583 edge-sealed vacuum insulated glazing. *Renewable Energy*, 135, pp.450-464.
584
- 585 [10]. Fang, Y., Eames, P.C., Norton, B. and Hyde, T.J., 2006. Experimental validation of a
586 numerical model for heat transfer in vacuum glazing. *Solar Energy*, 80(5), pp.564-577.
587
- 588 [11]. Collins, R.E. and Simko, T.M., 1998. Current status of the science and technology of
589 vacuum glazing. *Solar Energy*, 62(3), pp.189-213.
590
- 591 [12]. Zhao, J.F., Eames, P.C., Hyde, T.J., Fang, Y. and Wang, J., 2007. A modified pump-out
592 technique used for fabrication of low temperature metal sealed vacuum glazing. *Solar*
593 *Energy*, 81(9), pp.1072-1077.
594
- 595 [13]. Collins and Fischer, 1991. Evacuated glazing. *Solar Energy* 47 27-38.
596
- 597 [14]. Memon, S., 2013. Design, Fabrication and Performance Analysis of Vacuum Glazing Units
598 Fabricated with Low and High Temperature Hermetic Glass Edge Sealing Materials, PhD
599 Thesis, Loughborough University, UK, <https://dspace.lboro.ac.uk/2134/14562>.
600
- 601 [15]. Memon, S., Farukh, F., Eames, P.C. and Silberschmidt, V.V., 2015. A new low-temperature
602 hermetic composite edge seal for the fabrication of triple vacuum glazing. *Vacuum*, 120,
603 pp.73-82.
604
- 605 [16]. Memon, S. and Eames, P.C., 2017. Predicting the solar energy and space-heating energy
606 performance for solid-wall detached house retrofitted with the composite edge-sealed triple
607 vacuum glazing. *Energy Procedia*, 122, pp.565-570.
608
- 609 [17]. Fang, Y., Hyde, T.J., Arya, F., Hewitt, N., Wang, R. and Dai, Y., 2015. Enhancing the
610 thermal performance of triple vacuum glazing with low-emittance coatings. *Energy and*
611 *Buildings*, 97, pp.186-195.
612
- 613 [18]. Ghosh A., Norton B., Duffy A. 2016. Measured thermal performance of a combined
614 suspended particle switchable device evacuated glazing. *Applied Energy* 169, 469–480.
615
- 616 [19]. Rezaei S.D., Shannigrahi S., Ramakrishna S., 2017. A review of conventional, advanced,
617 and smart glazing technologies and materials for improving indoor environment. *Solar*
618 *Energy Materials and Solar Cells*. 159, 26-51.
619
- 620 [20]. Manz, H., Brunner, S. and Wullschlegel, L., 2006. Triple vacuum glazing: Heat transfer and
621 basic mechanical design constraints. *Solar Energy*, 80(12), pp.1632-1642.
622
- 623 [21]. Fang Y., Hyde T.J., Arya F., Hewitt N., 2013. A novel building component hybrid vacuum
624 glazing - a modeling and experimental validation. *ASHRAE Transactions* 119, 430-441.
625
- 626 [22]. Qingdao hengda glass technology co, ltd. 2019. Hd-glasscom. [Online]. [15 May 2019].
627 Available from: <http://www.hd-glass.com/en/about.aspx>
628
- 629 [23]. LandVac-Vacuum-glassnet. 2019. Vacuum-glassnet. [Online]. [10 April 2019]. Available
630 from: <https://www.vacuum-glass.net/>
631

- 632 [24]. Panasoniccom. 2019. Panasonic Newsroom Global. [Online]. [13 June 2019]. Available
633 from: <http://news.panasonic.com/global/press/data/2017/12/en171205-2/en171205-2.html>
634
- 635 [25]. NSG SPACIA, 2019. Pilkington NSG Hybrid Vacuum Glazing [Online]. [23rd May 2019].
636 Available from: [https://www.nsg.com/en/media/ir-updates/announcements-2018/super-](https://www.nsg.com/en/media/ir-updates/announcements-2018/super-spacia-award)
637 [spacia-award](https://www.nsg.com/en/media/ir-updates/announcements-2018/super-spacia-award)
638
- 639 [26]. EN 673, 2011. Glass in building – Determination of thermal transmittance (U-value) –
640 Calculation method. Brussels: European Committee for Standardization (CEN).
641
- 642 [27]. Memon, S., 2017. Experimental measurement of hermetic edge seal's thermal conductivity
643 for the thermal transmittance prediction of triple vacuum glazing. Case studies in thermal
644 engineering, 10, pp.169-178.
645
- 646 [28]. Duffie, J.A. and Beckman, W.A., 1991. Solar engineering of thermal processes (pp. 770-
647 772). New York: Wiley.

Journal Pre-proof

This work funded by the Pump-Prime project of Coventry University and the self-initiated UK China industrial research collaboration is original research which is the further development of our previous research work, does not conflict with the interest of any third parties.

Corresponding Author: Yueping Fang

Address: Coventry University, Centre for Research in Built and Natural Environment, School of Energy, Construction and Environment, Priory Street, Coventry, CV1 5FB, UK

Journal Pre-proof

Highlights

- Validated thermal performance of air-vacuum layered triple glazed window (IVW) is reported
- Indoor/outdoor position of vacuum layer influences solar thermal performance.
- Influences of dynamic solar insolation on thermal performance of the IVW are analysed.
- In winter conditions, the U-value of IVW on warm-side, i.e. $0.33 \text{ Wm}^{-2}\text{K}^{-1}$, is lower than cold-side, i.e. $0.49 \text{ Wm}^{-2}\text{K}^{-1}$.